



ELSEVIER

Available online at [www.sciencedirect.com](http://www.sciencedirect.com)

SCIENCE @ DIRECT®

Coastal Engineering 49 (2003) 291–305

**Coastal  
Engineering**  
An International Journal for Coastal,  
Harbour and Offshore Engineers

[www.elsevier.com/locate/coastaleng](http://www.elsevier.com/locate/coastaleng)

# Phase-decoupled refraction–diffraction for spectral wave models

L.H. Holthuijsen<sup>a,\*</sup>, A. Herman<sup>b</sup>, N. Booij<sup>a,1</sup>

<sup>a</sup>Faculty of Civil Engineering and Geosciences, Delft University of Technology, Stevinweg 1, 2628CN, Delft, The Netherlands

<sup>b</sup>Institute of Oceanography, University of Gdansk, Pilsudskiego 46, 81-378, Gdynia, Poland

Received 13 November 2002; accepted 17 July 2003

## Abstract

Conventional spectral wave models, which are used to determine wave conditions in coastal regions, can account for all relevant processes of generation, dissipation and propagation, except diffraction. To accommodate diffraction in such models, a phase-decoupled refraction–diffraction approximation is suggested. It is expressed in terms of the directional turning rate of the individual wave components in the two-dimensional wave spectrum. The approximation is based on the mild-slope equation for refraction–diffraction, omitting phase information. It does therefore not permit coherent wave fields in the computational domain (harbours with standing-wave patterns are excluded). The third-generation wave model SWAN (Simulating WAVes Nearshore) was used for the numerical implementation based on a straightforward finite-difference scheme. Computational results in extreme diffraction-prone cases agree reasonably well with observations, analytical solutions and solutions of conventional refraction–diffraction models. It is shown that the agreement would improve further if singularities in the wave field (e.g., at the tips of breakwaters) could be properly accounted for. The implementation of this phase-decoupled refraction–diffraction approximation in SWAN shows that diffraction of random, short-crested waves, based on the mild-slope equation can be combined with the processes of refraction, shoaling, generation, dissipation and wave–wave interactions in spectral wave models.

© 2003 Elsevier B.V. All rights reserved.

**Keywords:** Wave prediction; Spectral wave model; Wave propagation; Refraction; Diffraction; Numerical modelling

## 1. Introduction

Waves approaching a coastline may refract and diffract due to the presence of shoals and channels or obstacles such as islands, headlands, or breakwaters.

The effects of *refraction* are readily accounted for in phase-averaged (i.e., spectral) wave models. These models can also account for the generation, dissipation and wave–wave interactions of the waves in deep and shallow water (e.g., Booij et al., 1999; Benoit et al., 1996). However, this type of model does not account for *diffraction*. The effects of diffraction are traditionally computed with phase-resolving models such as mild-slope models (e.g., Battjes, 1968; Schönfeld, 1971; Holthuijsen, 1971; Berkhoff, 1972; Radder, 1979; Booij, 1981; Kirby, 1986) or Boussinesq models (e.g., Peregrine, 1966; Madsen and Sørensen, 1992; Li and Zhan, 2001). However, these models do

\* Corresponding author. Tel.: +31-15-2784803; fax: +31-15-274842.

E-mail addresses: l.holthuijsen@ct.tudelft.nl (L.H. Holthuijsen), herman@sat.ocean.univ.gda.pl (A. Herman), nico.booij@freeler.nl (N. Booij).

<sup>1</sup> Now at Digital Hydraulics, Wilgewinde 22, 3317 ME, Dordrecht, The Netherlands.

not, or only to a limited degree, account for the generation, dissipation and wave–wave interactions of the waves. A combination of the two types of model capabilities would obviously be most convenient: add diffraction to a spectral model *or* add the generation, dissipation and wave–wave interactions of waves to a phase-resolving model (mild-slope or Boussinesq). Adding diffraction to a spectral model has the advantage that (a) large-scale computations remain perfectly feasible (as long as the required high spatial resolution in the diffraction regions are retained, e.g., by nesting or by using a variable-resolution grid; in contrast to this, phase-resolving models require a prohibitively high spatial resolution over the entire computational region), (b) the random, short-crested character of the waves is inherent (in contrast to this, mild-slope models would require multiple runs) and (c) the formulations for all processes of generation and dissipation and wave–wave interactions are included (in contrast to this, phase-resolving models do not include all of these).

One approach to add diffraction to a spectral model would be to mimic diffraction with spatial or spectral diffusion (e.g., Resio, 1988; Booij et al., 1997; Mase et al., 2001). This approach has been shown to simulate some of the diffraction effects, but either the effects are limited (e.g., the diffraction induced turning of the wave direction is not simulated) or the numerical schemes are not stable. Another approach is to add the diffraction-induced turning rate of the waves (obtained from the mild-slope equation) to a spectral model. This was suggested by Booij et al. (1997) and Rivero et al. (1997). In the present study this option is implemented in the third-generation spectral wave model SWAN (Booij et al., 1999). Computational results are compared to analytical solutions, results of conventional refraction–diffraction models and observations.

## 2. The mild-slope equation

Consider a harmonic wave with complex wave function  $\xi = a \exp(i\psi)$ , where  $Re(\xi e^{i\omega t})$  is the surface elevation as it varies in space and time,  $a = a(x, y)$  is the (stationary) amplitude and  $\psi = \psi(x, y)$  is the (stationary) phase function. In the linear theory of surface gravity waves over a mildly sloping bottom, the

propagation of this wave is given by the mild-slope equation (Berkhoff, 1972):

$$\nabla \cdot cc_g \nabla \xi + \kappa^2 cc_g \xi = 0 \quad (1)$$

where  $c = \omega/\kappa$  and  $c_g = \partial\omega/\partial\kappa$  and the separation parameter  $\kappa$  is determined from  $\omega^2 = g\kappa \tanh(\kappa d)$  (where  $g$  is gravitational acceleration and  $d$  is water depth (e.g., Dingemans, 1997)). In the absence of diffraction,  $c$  and  $c_g$  would be the phase speed and the group velocity respectively and  $\kappa$  would be equal to the wave number  $k$  (the magnitude of the spatial gradient of the phase function  $\psi$ ):  $\kappa = k = |\nabla\psi|$ . By multiplying the mild-slope equation with the complex conjugate of  $\xi$  and then taking the imaginary part, we obtain an energy balance equation, which for a constant frequency  $\omega$  (a basic assumption for the mild-slope equation), reduces to

$$\nabla \left[ \frac{k}{\kappa} c_g a^2 \right] = 0 \quad (2)$$

This energy balance equation shows that, in the presence of diffraction the energy propagation speed in geographic space, is

$$C_g = \frac{k}{\kappa} c_g \quad (3)$$

By substituting the wave function into the mild-slope equation it is readily shown that the magnitude of the gradient of the phase function in the presence of diffraction is given by

$$k^2 = \kappa^2 + \frac{\nabla \cdot (cc_g \nabla a)}{cc_g a} \quad (4)$$

If diffraction is ignored (i.e., the variation in amplitude is taken to be zero), the second term on the right-hand-side of Eq. (4) vanishes and this equation reduces to  $k = \kappa$ . This second term therefore represents diffraction in the phase function  $\psi$ . Denoting the diffraction parameter  $\delta_a$  as

$$\delta_a = \frac{\nabla \cdot (cc_g \nabla a)}{\kappa^2 cc_g a} \quad (5)$$

the diffraction-corrected phase speed  $C$  is

$$C = \omega/k = c(1 + \delta_a)^{-1/2} \quad (6)$$

and the diffraction-corrected group velocity is

$$C_g = c_g(1 + \delta_a)^{1/2} \quad (7)$$

The spatial rate of directional turning can be derived for a spatially varying phase speed, without assuming that the variations are induced by refraction. The derivation can be formal, using general mathematical properties of the phase function (e.g., [Dingemans, 1997](#); his Eq. (2.94)). As an alternative, the following derivation is based on a more physically oriented geometric argument. Consider in an arbitrary situation, a line of equal phase (iso-phase line) of the wave, along which the phase speed varies ([Fig. 1](#)). A right-turning system of orthogonal  $m, s$  coordinates is used with  $m$  oriented along the iso-phase line. Two points, A and B on the iso-phase line, separated by distance  $\Delta m$ , move in a time interval  $\Delta t$  normal to the iso-phase line (along an orthogonal or wave ray) over a distance  $\Delta s_A = c\Delta t$  and  $\Delta s_B = (c + \Delta c)\Delta t$ , respectively. The corresponding directional turning of the iso-phase line is  $\Delta\theta = (\Delta s_A - \Delta s_B)/\Delta m$ . The spatial rate of direc-

tional turning  $\Delta\theta/\Delta s$  (per unit distance in the wave direction, i.e., along the wave ray) is therefore  $\Delta\theta/\Delta s = -\Delta c\Delta t/\Delta m\Delta s$ . Or, since  $\Delta s = c\Delta t$ ,  $\Delta\theta/\Delta s = -(\Delta c/c)/\Delta m$ . For infinitesimally small differences, this is

$$\frac{\partial\theta}{\partial s} = -\frac{1}{c} \frac{\partial c}{\partial m} \quad (8)$$

With  $c = \omega/k$  and  $\omega = \text{constant}$  substituted in this Eq. (8), this turning rate can also be written as

$$\frac{\partial\theta}{\partial s} = \frac{1}{k} \frac{\partial k}{\partial m} \quad (9)$$

or in terms of the separation parameter  $\kappa$  (substituting Eq. (4) in Eq. (9)),

$$\frac{\partial\theta}{\partial s} = \frac{1}{k} \frac{\partial k}{\partial m} = \frac{1}{\kappa} \frac{\partial \kappa}{\partial m} + \frac{1}{2(1 + \delta_a)} \frac{\partial \delta_a}{\partial m} \quad (10)$$

If diffraction is ignored,  $\delta_a = 0$  and the turning rate reduces to the commonly used turning rate for refraction only:

$$\frac{\partial\theta}{\partial s} = \frac{1}{k} \frac{\partial k}{\partial m} = \frac{1}{\kappa} \frac{\partial \kappa}{\partial m} \quad (11)$$

### 3. The spectral energy balance

In the absence of diffraction and currents, the spectral energy balance equation, which is the basic equation of spectral wave models, is (e.g., [Komen et al., 1994](#))

$$\frac{\partial E}{\partial t} + \frac{\partial c_x E}{\partial x} + \frac{\partial c_y E}{\partial y} + \frac{\partial c_\theta E}{\partial \theta} = S \quad (12)$$

where  $E = E(\omega, \theta)$  is the energy density of the waves as a function of frequency  $\omega$  and direction  $\theta$ . The generation, dissipation, and wave-wave interactions of the waves are represented by the source term  $S = S(\omega, \theta)$ . Since inclusion of this term is not relevant for this study, we will ignore it, so that  $S(\omega, \theta) = 0$ . The first term on the left-hand side represents the local rate of change of energy density ( $t$  is time), the second and third term represent rectilinear propagation in the horizontal, flat plane ( $x, y$ ; propagation on a sphere is ignored here). The fourth term represents propagation

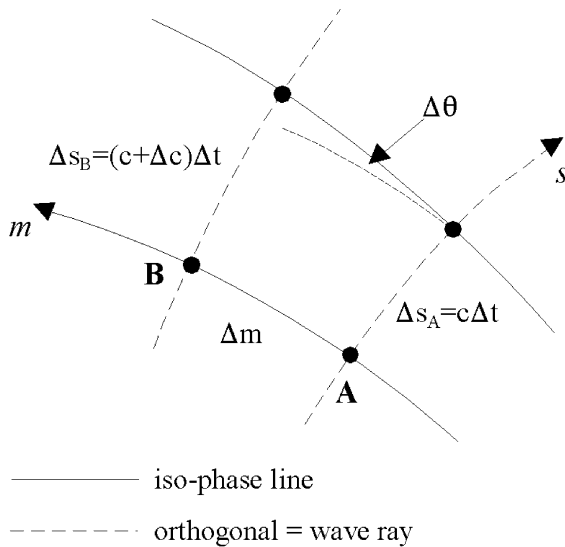


Fig. 1. The directional turning of an iso-phase line and corresponding orthogonals (wave rays).

in spectral direction space (refraction). The propagation speeds  $c_x$ ,  $c_y$  are the  $x$ -,  $y$ -component of the group velocity  $c_g$  respectively and  $c_\theta$  is the rate of directional turning (propagation speed in  $\theta$ -dimension). (The dependencies on  $x$ ,  $y$  and  $t$  have been ignored in the notation for the sake of brevity.) These propagation speeds are taken from the linear theory of surface gravity waves without the effects of diffraction (e.g., Mei, 1983; Dingemans, 1997). To add diffraction, note that the turning rate  $c_\theta$  is the rate of directional change of a single wave component as it travels along the wave ray with the group velocity. It is readily obtained from the spatial turning rate  $\partial\theta/\partial s$ . As the wave energy travels along the ray over a distance  $\Delta s$  in a time interval  $\Delta t$ , it turns over an angle  $\Delta\theta$ . The spatial rate of turning is then  $\Delta\theta/\Delta s$ . Since the distance  $\Delta s = c_g \Delta t$ , it follows that the temporal rate of turning  $\Delta\theta/\Delta t = c_g \Delta\theta/\Delta s$ . Taking the infinitesimal limits, denoting the temporal rate of turning as  $c_\theta$  and substituting Eq. (10), gives

$$c_\theta = c_g \frac{\partial\theta}{\partial s} = c_g \left( \frac{1}{k} \frac{\partial k}{\partial m} \right) \quad (13)$$

Adding diffraction to the energy balance equation involves only replacing  $c_g$  by  $C_g$  and  $c_\theta$  by  $C_\theta$  in the spectral energy balance of Eq. (12).

$$C_\theta = C_g \frac{\partial\theta}{\partial s} = C_g \left( \frac{1}{\kappa} \frac{\partial\kappa}{\partial m} + \frac{1}{2(1 + \delta_a)} \frac{\partial\delta_a}{\partial m} \right) \quad (14)$$

These expressions for  $C_g$  and  $C_\theta$  are formulated in terms of the diffraction parameter  $\delta_a$ , which is expressed in terms of the amplitude of a harmonic wave and not in terms of the spectral density  $E(\sigma, \theta)$ . Unfortunately, formulations in terms of  $E(\sigma, \theta)$  are not available but it seems reasonable to replace the normalised derivatives of amplitude  $a$  in these expressions by the normalised derivatives of the square root of the energy density,  $\sqrt{E} = \sqrt{E(\sigma, \theta)}$  (the more so as both are normalised), so that  $\delta_a$  is replaced by  $\delta_E$ .

$$\delta_E = \frac{\nabla \cdot (cc_g \nabla \sqrt{E})}{\kappa^2 cc_g \sqrt{E}} \quad (15)$$

Including this diffraction term in the expression of Eq. (14) for the turning rate seems to be a straight-

forward expansion of the energy balance equation. But it is not. The energy balance equation does not account for the phase evolution of the waves, whereas the mild-slope equation does: replacing the amplitude  $a = a(x, y)$  with the energy density  $E(\sigma, \theta; x, y)$  removes phase-information and therefore decouples the phases spatially. We will therefore refer to this approximation as the phase-decoupled refraction–diffraction approximation. (The corresponding expressions for the propagation speeds in the presence of currents are given in Appendix A) The most important effect of decoupling the waves in practical applications seems to be that standing wave patterns are not accounted for (i.e., nodal wave patterns are absent). This characteristic is shared with the parabolic refraction–diffraction approximation of the mild-slope equation, albeit for other underlying reasons. In the parabolic approximation, waves cannot reflect and propagate against the incident wave direction (e.g., Radder, 1979; Booij, 1981), which implies that standing wave patterns cannot be properly represented in the parabolic approximation. In the present phase-decoupled approximation, waves can reflect and propagate against the incident wave direction but phase coupling between the incident wave and its reflection (required to represent a nodal pattern) is not possible.

With this addition of phase-decoupled diffraction, the spectral energy balance equation changes from a second-order differential equation to a fourth-order equation: the refraction term on the left-hand-side of Eq. (12) contains a first-order spectral derivative of  $c_\theta$ , which itself contains a first-order spatial derivative. The diffraction parameter  $\delta_E$  adds a second-order spatial derivative of  $\sqrt{E(\sigma, \theta)}$ . By separating the numerical treatment of diffraction (see below) from the numerical treatment of refraction, a conventional spectral model for refraction can be expanded to include this approximation of diffraction.

#### 4. Numerical implementation

The expressions for the group velocity  $C_g$  of Eq. (7) and the directional turning rate  $C_\theta$  of Eq. (14) with  $\delta_E$  from Eq. (15) have been implemented in the SWAN model of Booij et al. (1999). This third-generation wave model is based on the action balance equation, which reduces to the energy balance equation in the

absence of currents. Ignoring the generation, dissipation, and wave–wave interactions, reduces the basic equation of SWAN further to Eq. (12) with  $S(\omega, \theta) = 0$ . In some of the following validation cases, we will use the option in SWAN for reflection against obstacles (linear reflection elements with one dimension smaller than the grid resolution). With this option, the wave energy of each wave component reflects in a specular mode off an obstacle.

For the propagation in geographic space (which accounts for rectilinear propagation and shoaling), an iterative, up-wind, implicit scheme with third-order diffusion is used in SWAN (the SORDUP-scheme; Rogers et al., 2002). The (near) absence of numerical diffusion in this scheme ensures that practically all spreading and smoothing effects in the wave field are not due to numerical diffusion (which is sometimes suggested to simulate diffraction, e.g., Resio, 1988). For propagation in spectral space (which accounts for refraction), an implicit, second-order upwind scheme, which is supplemented with a central scheme, is used (Booij et al., 1999). It too has very little numerical diffusion and does therefore also not simulate diffraction.

The diffraction effect is implemented in SWAN by adding the diffraction parameter  $\delta_E$  to the expressions for the group velocity components  $c_x$ ,  $c_y$  and to the turning rate  $c_\theta$  (i.e., the refraction term) in these propagation schemes. In each of the iterations of the original propagation scheme, the second-order derivative  $\nabla \cdot (CC_g \nabla \sqrt{E(\sigma, \theta)})$  in the expression of  $\delta_E$  is obtained with a simple, second-order central scheme based on the results of the previous iteration. For the  $x$ -dimension the estimation is

$$\begin{aligned} & \left[ \frac{\partial}{\partial x} \left( CC_g \frac{\partial \sqrt{E}}{\partial x} \right) \right]^n \\ & \cong \frac{1}{2\Delta x^2} \left[ \left\{ (CC_g)_i + (CC_g)_{i-1} \right\} \sqrt{E_{i-1}} \right. \\ & \quad \left. - \left\{ (CC_g)_{i-1} + 2(CC_g)_i + (CC_g)_{i+1} \right\} \sqrt{E_i} \right. \\ & \quad \left. + \left\{ (CC_g)_i + (CC_g)_{i+1} \right\} \sqrt{E_{i+1}} \right]^{n-1} \quad (16) \end{aligned}$$

where  $i$  is a grid counter in  $x$ -dimension and the superscript  $n$  indicates iteration number. For the  $y$ -dimension, the expression is identical, with  $y$  replac-

ing  $x$ . The estimation of  $\delta_E$  is thus based on the values of the energy density  $E$  obtained from the preceding iteration in the geographic propagation scheme (the value of  $\delta_E$  is cut off at the low side at  $-1$  to avoid imaginary propagation speeds; there is no upper bound). For models with a variable geographic resolution (optional in SWAN), the numerical approximation of the gradients needs to account for different values of  $\Delta x$  and  $\Delta y$  on either side of the central grid point in the scheme (not available in the present version of SWAN). The advantage of a variable-resolution grid is that the model can be based on a high spatial resolution where diffraction requires this (near obstacles) and on a coarser resolution where such high resolution is not required. Diffraction is thus computed in the entire computational domain with high resolution only where needed. At the boundaries of the computational domain (coast, obstacle or open boundaries) first-order spatial gradients in SWAN are set at zero. Open boundaries should therefore be chosen such that diffraction near these boundaries can be ignored, i.e., the gradients should be small there. At the coast or at an obstacle, the second-order gradients are approximated with the assumption of a horizontal first-order gradient at the coast or the obstacle. Various other boundary conditions were tried but the effects on the computational results of this study (see below) were barely noticeable.

The discretization of the gradients with the finite difference scheme of Eq. (16), in terms of the values of  $\sqrt{E(\sigma, \theta)}$  in neighbouring points in the  $x$ - and  $y$ -dimension, seems trivial but the following shows that it is not. Diffraction of random, short-crested waves can also be computed as the superposition of solutions for a large number of incident monochromatic, unidirectional waves, each computed independently with the mild-slope equation. In each such computation, the spatial gradient is taken of the amplitude of the monochromatic wave. The direction of such a monochromatic wave varies geographically so that for each grid point in the computational domain, the wave energy in neighbouring grid points propagates in slightly different directions. The spatial gradient of  $\sqrt{E(\sigma, \theta)}$  in the present approach (estimated from these neighbouring points) should therefore also be taken at these slightly different directions. Instead, Eq. (16) states that at these grid points the same direction

is to be taken as in the central grid point. In the extreme case of a semi-infinite breakwater, the corresponding error in direction can be estimated from the fact that in the shadow zone behind the breakwater, the wave crests are nearly circular and centred at the tip of the breakwater. The difference in wave direction  $\Delta\theta$  at two neighbouring grid points is then approximately  $\Delta\theta \cong \Delta x/r$  where  $\Delta x$  is the spatial resolution and  $r$  is the distance to the tip of the breakwater. To reduce this error to acceptable proportions would require that  $E(\sigma, \theta) \cong E(\sigma, \theta + \Delta\theta)$ . This implies that  $\Delta\theta$  be small compared to the width  $\sigma_\theta$  of the directional distribution of the wave spectrum, i.e.,  $\Delta\theta = \Delta x/r \ll \sigma_\theta$ . For wind waves, with a directional width of typically  $30^\circ$ , this is only true for distances of more than  $10\Delta x$  to  $20\Delta x$  from the breakwater tip. With a resolution of  $\Delta x = 1/5$  to  $1/10$  of the wavelength (typical for refraction–diffraction models), this implies that this approximation is reasonable only at a distance larger than one or two wavelengths from the breakwater tip. However, at such a distance, the gradients in the wave field are usually small and diffraction need no longer be considered (i.e., the local diffraction-induced turning of the wave direction). For swell, with a directional width of  $10^\circ$  or so, the distance would be even larger. Nevertheless, the computations of this study were tried with  $\sqrt{E(\sigma, \theta)}$  but they converged so slowly as to be impracticable. They will not be considered here. To avoid these problems, the direction-integrated spectral density  $E(\sigma)$  is taken instead of  $E(\sigma, \theta)$ , but only to estimate the value of  $\delta_E$ .

In early computations of this study, the wave fields often showed slight “wiggles” in geographic space with a wavelength of about  $2\Delta x$  in  $x$ -direction (or  $2\Delta y$  in  $y$ -direction). These unduly affected the estimations of the gradients that were needed to compute the diffraction parameter  $\delta_E$ . The wave field was therefore smoothed with the following convolution filter:

$$E_{ij}^n = E_{ij}^{n-1} - 0.2 \times [E_{i-1,j} + E_{i,j-1} - 4E_{i,j} + E_{i+1,j} + E_{i,j+1}]^{n-1} \quad (17)$$

where  $i$  is a grid counter in  $x$ -dimension, the superscript  $n$  indicates iteration number (i.e., iteration of the

convolution cycle). The width of this filter (standard deviation) in  $x$ -direction  $\varepsilon_x$ , when applied  $n$  times is

$$\varepsilon_x \approx \frac{1}{2} \sqrt{3n} \Delta x \quad (18)$$

In the computations of the present study,  $n=6$  was found to be an optimum value (smallest value of  $n$  for which the computations, with spatial resolution  $1/5$  to  $1/10$  of the wavelength, remained numerically stable), so that  $\varepsilon_x \approx 2\Delta x$  in the present study. For the  $y$ -dimension, the expressions are identical, with  $y$  replacing  $x$ . Note that this smoothing is only applied to compute the diffraction parameter  $\delta_E$ . For all other computations the wave field was not smoothed.

Breakwaters or other obstacles will induce discontinuities in the wave field and corresponding singularities in the diffraction-induced turning rate of the waves. The finite difference scheme of Eq. (16) is not suited to approximate these discontinuities and singularities. Estimating the gradients at these locations therefore requires a different numerical treatment. This was not investigated in any depth but to illustrate the significance of these discontinuities and singularities, an ad-hoc approach was taken by enhancing the value of  $c_\theta$  as computed with the above technique by a factor 50, but only at the one grid point in the shadow zone behind the corner point of the obstacle that is nearest to the corner point (e.g., the tip of a breakwater in case of a breakwater). This grid point may be different for different wave directions as each wave direction casts its own shadow. Trial and error showed that larger enhancements sent too much energy into the deep shadow area behind the breakwaters whereas much lower values were ineffective.

## 5. Verification

### 5.1. Introduction

As stated earlier, the aim of adding the above phase-decoupled refraction–diffraction approximation to the spectral energy balance is, to obtain a reasonable estimate of diffraction effects in large-scale computations (size of computational domain is dozens of wave lengths or more) in which the waves are assumed to be random, short-crested and non-coher-

ent. To verify the present approach would require observations or superior computations with convincing diffraction effects in such conditions. However, to the best of our knowledge, these are not available. We therefore consider instead small-scale computations (size of computational domain at most a few wave lengths) for which such observations or superior computations are available. However, even at such small scales, diffraction is barely noticeable for random, short-crested wind waves (e.g., wind sea conditions with a JONSWAP spectrum, Hasselmann et al., 1973, and  $30^\circ$  directional spreading). We therefore consider situations with monochromatic, unidirectional waves, and occasionally long-crested, random waves. These verification conditions are well outside the intended range of applications. It implies our confidence that if the model performs reasonably well in these conditions, it will almost certainly perform reasonably well within the proper range of applications where diffraction is significantly less relevant.

We consider two types of academic cases. The first is a situation without land or obstacles, where diffraction is induced by variations in the wave field due to extreme refraction (over an elliptical shoal). The second type is one in which a breakwater induces diffraction. We consider laboratory measurements, analytical solutions and numerical solutions of parabolic refraction–diffraction models.

## 5.2. Elliptical shoal

Vincent and Briggs (1989) measured waves propagating across an elliptical shoal with major and minor radii of 3.96 and 3.05 m, respectively (at the bottom of a laboratory wave tank; Fig. 2). The maximum height of the shoal above the bottom is 0.305 m and the largest water depth is 0.457 m. The waves propagate across this shoal with significant refraction effects (probably including caustics) with corresponding wave amplitude variations. These variations induce diffraction effects, which will tend to smooth the wave amplitude pattern. We will consider two cases: one with monochromatic, unidirectional waves and one with random, long-crested waves.

The wave fields have been computed with SWAN, with and without diffraction. SWAN is fundamentally formulated in terms of a spectrum with finite directional bandwidth. The waves can therefore not be

exactly unidirectional as in the observations. (Such finite bandwidth would also be required in frequency space in the presence of an ambient current to allow frequency shifting. However, in the absence of such currents, as is the case here, monochromatic waves can be modelled with one frequency in SWAN).

### 5.2.1. The monochromatic-wave case (the $\delta$ -spectrum)

The incident waves for the monochromatic case are approximated with a spectrum with one frequency and a very narrow Gaussian directional distribution around the mean direction. The incident wave height and period are 0.055 m and 1.30 s, respectively. The directional spreading is  $\sigma_\theta = 1.5^\circ$  (defined as in Kuik et al., 1988) and the directional resolution in the computations  $\Delta\theta = 0.25^\circ$ . We will refer to this spectrum as the  $\delta$ -spectrum. The spatial resolution is  $\Delta x = \Delta y = 0.2 \text{ m} \approx 0.08L$  ( $L$  = wave length).

The computed wave field is compared with the observations of Vincent and Briggs (1989) and with the computational results of Panchang et al. (1990; which they obtained with their parabolic refraction–diffraction model). Since the case is symmetrical around the centre line of the shoal, the observations and computational results are shown only in one half of the tank (different half for different results; Fig. 2). The observations are presented here with the normalised wave height in plan view and along two lines: the centre line of the tank and a line normal to the centre line through the location with minimum wave height (slightly different location in the different models). Inspection of the computational results of SWAN in Fig. 2 shows that adding the phase-decoupled refraction–diffraction approximation to the conventional refraction computation, spreads the effect of the shoal over a slightly larger area (particularly in the lateral direction). It does not affect the maximum value of the wave height and it only slightly increases the minimum wave height. The values of the maximum and minimum wave height are reasonably well reproduced with the phase-decoupled approximation (normalised values: 2.2 computed vs. 2.4 observed and 0.6 computed vs. 0.6 observed, respectively). The parabolic approximation of Panchang et al. (1990) gives a better estimate of the observed maximum wave height (2.4 vs. 2.4; lower panel of Fig. 2) but not for the minimum wave height (0.2 vs. 0.6; lower panel of Fig. 2). The wave patterns

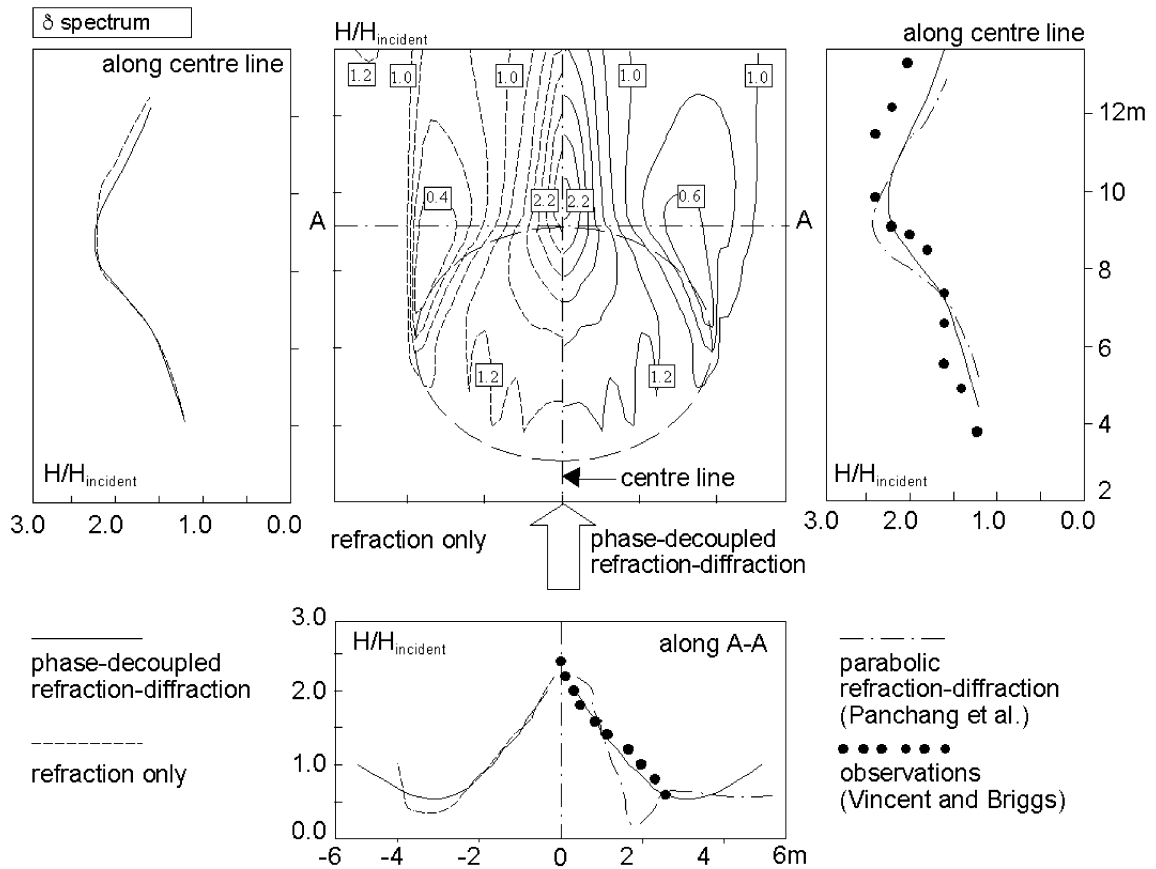


Fig. 2. Normalised wave height (local wave height divided by incident wave height) for unidirectional, monochromatic waves propagating from bottom to top (in this figure) over an elliptical shoal. Since the computational results are symmetric around the centre line, they are shown for half the tank (left side=refraction only; right side=phase-decoupled refraction–diffraction). Line (A–A) through the location of minimum wave height. Comparison with the observations of Vincent and Briggs (1989; inferred from their figures) and the parabolic refraction–diffraction approximation of Panchang et al. (1990; inferred from their figures).

of the phase-decoupled approximation and of the parabolic approximation differ significantly outside the area of observation (not shown here). In this outer area where only computational results are available, the results of the parabolic approximation show a line of minimum wave height (normalised wave height as low as 0.4), starting just outside the area that is shown in Fig. 2, radiating in a direction away from the centre of the shoal under an angle of roughly  $30^\circ$  (relative to the incident wave direction). This line of minimum wave height is missing in the phase-decoupled approximation. No judgement is possible without observations but the pattern in the parabolic approximation may well be realistic as it also occurs in observations

by Berkhoff (1972) and in the Boussinesq model of Li and Zhan (2001) for wave propagation over a (different) shoal.

#### 5.2.2. The random-wave case (the narrow spectrum)

The above case is also considered for long-crested incident waves. These are approximated in SWAN with the narrow JONSWAP spectrum that was used in the laboratory experiments of Vincent and Briggs (1989; peak enhancement factor  $\gamma=20$  and directional width  $\sigma_\theta \approx 10^\circ$ ). The incident significant wave height is 0.0254 m and the peak period is 1.30 s. The computational results are shown in Fig. 3. The effect of adding the phase-

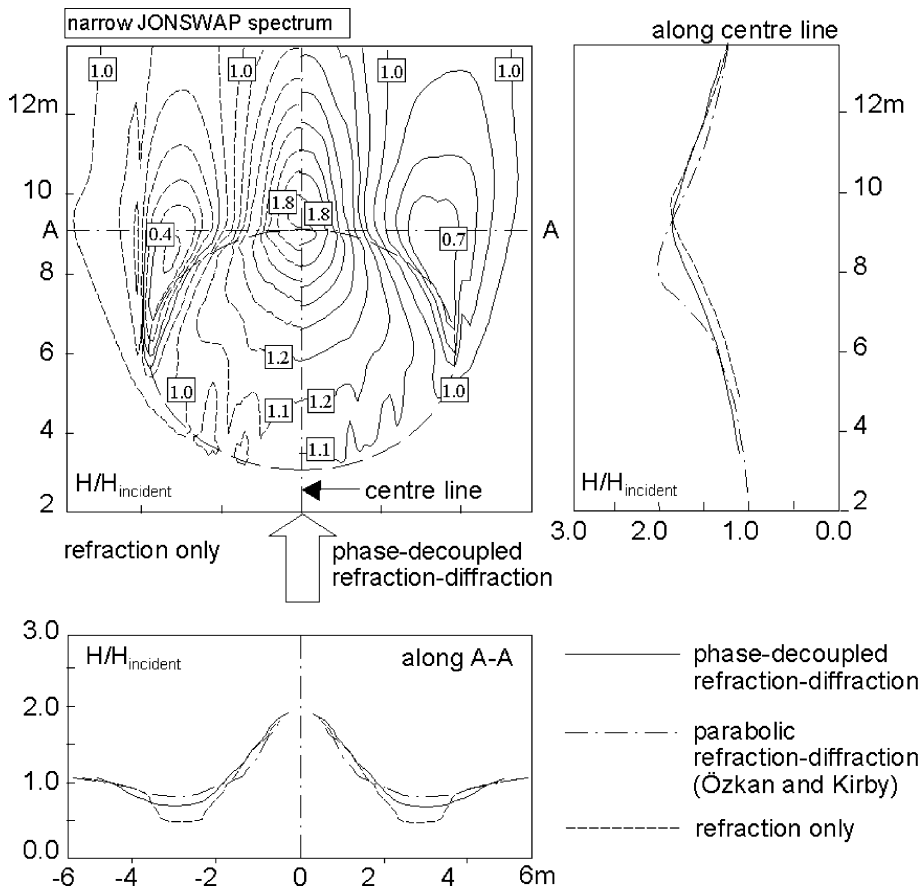


Fig. 3. Normalised wave height (local wave height divided by incident wave height) for waves with a narrow JONSWAP spectrum propagating from bottom to top (in this figure) over an elliptical shoal. Since the computational results are symmetric around the centre line, they are shown for half the tank (left side = refraction only; right side = phase-decoupled refraction–diffraction). Comparison with the parabolic refraction–diffraction solution of Özkan and Kirby (1993; inferred from their figures) along the centre line and line A–A (at end of shoal).

decoupled approximation is essentially the same as in the above monochromatic case. The phase-decoupled approximation hardly affects the maximum wave height but it increases the minimum wave height (normalised value from 0.4 to 0.7). These results are reasonably close to the solution of the parabolic approximation of Özkan and Kirby (1993), as shown in Fig. 3.

### 5.3. Breakwaters

Occasionally a breakwater may occur in the computational domain. To estimate the effect of this in the present approach, we consider the classical case of a semi-infinite breakwater and a gap in an infinitely

long breakwater. As noted earlier, such obstacles will induce discontinuities in the wave field and corresponding singularities in the diffraction-induced turning rate of the waves. This aspect of the computations will be addressed separately.

#### 5.3.1. Semi-infinite breakwater

Consider a situation with a semi-infinite, infinitely thin, vertical, rigid, fully reflecting straight screen (breakwater) in an infinite body of water with constant depth. Unidirectional, monochromatic waves approach the breakwater perpendicularly from one side (Fig. 4). The analytical solution for this case (due to Sommerfeld, 1896; see also Lamb, 1932) is given in Fig. 4 in terms of the normalised wave height (local

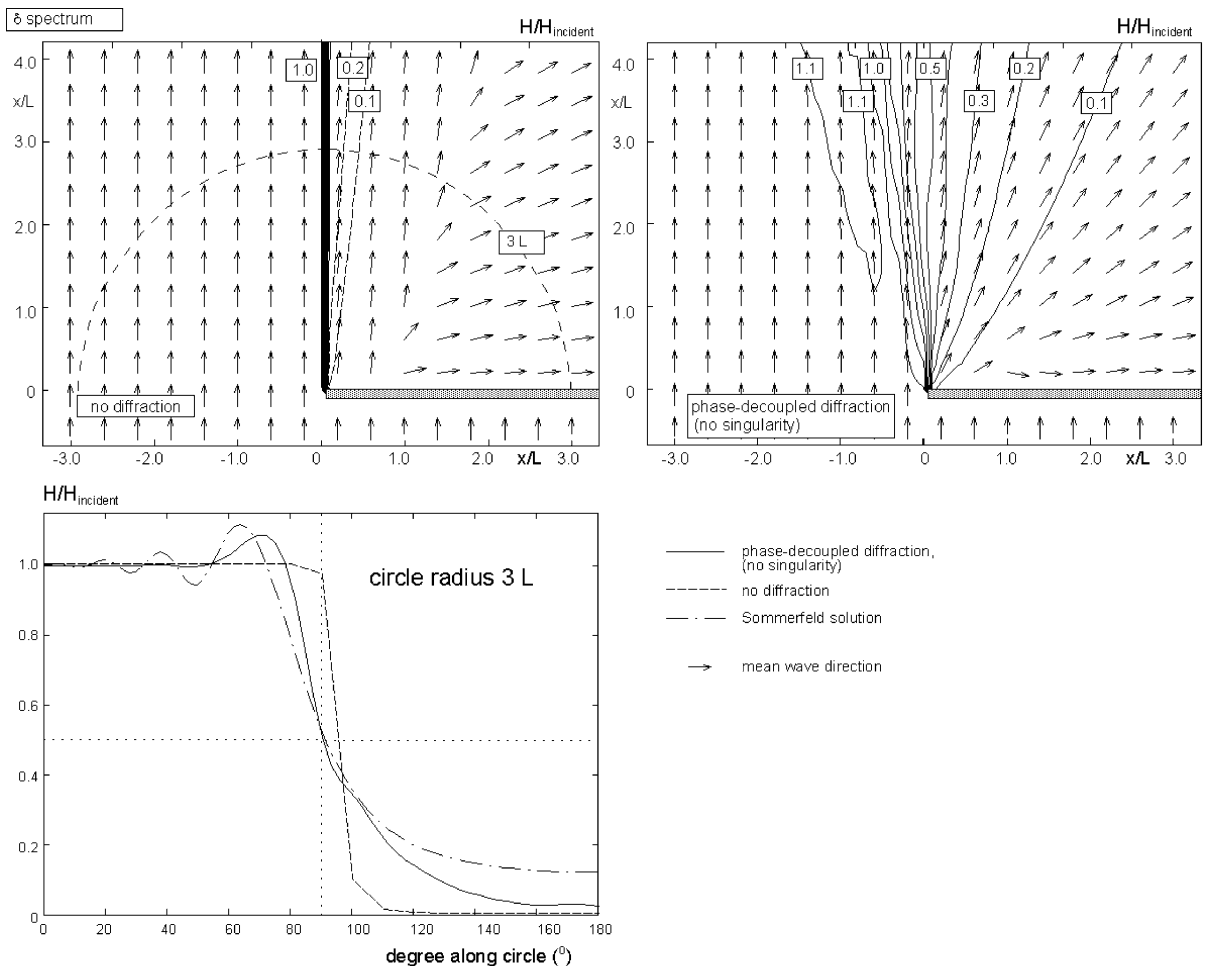


Fig. 4. Normalised wave height (local wave height divided by incident wave height) of unidirectional, monochromatic waves propagating around a semi-infinite, straight breakwater. Upper left panel=no diffraction, upper right panel=phase-decoupled diffraction (no singularity accounted for). Lower panel=circular-section at 3.0 times wavelength  $L$ , including comparison with analytical solution of Sommerfeld.

wave height/incident wave height). In the SWAN computations the breakwater is fully reflecting and the waves are approximated with the same  $\delta$ -spectrum as above. It is obvious from the SWAN results (Fig. 4) that without diffraction, SWAN does not properly reproduce the Sommerfeld solution. Only a small fraction of the energy penetrates in the area behind the breakwater. This is essentially due to some numerical diffusion, illustrating the relatively small numerical diffusion of the propagation schemes in SWAN. Obviously, the wave direction in that region is the (spectral) direction of this diffused energy. Any energy above this level in the following diffraction

computations must be due to the diffraction approximation that is added in these computations. With the phase-decoupled refraction–diffraction approximation included (but without explicitly accounting for the singularity at the tip of the breakwater), SWAN reproduces the Sommerfeld solution reasonably well near the shadow line and in the exposed region and certainly much better than without diffraction (Fig. 4). Even the overshoot on the exposed side of the shadow line is reproduced to some extent. The largest deviations occur in the deep-shadow region (where normalised wave height  $< 0.3$ , i.e., less than 10% of the incident wave energy). The wave directions too are

well reproduced (even deep inside the shadow area where the error is less than  $5^\circ$ , not shown here). These computations were for unidirectional waves. For short-crested waves for which spectral wave models such as SWAN are basically intended, the diffraction effects reduce considerably in this case, both in the Sommerfeld solution (superposition for a large number of unidirectional waves) and in the phase-decoupled solution (computations were made with

spectral directional widths of  $10^\circ$  and more; results not shown here). However, also in these cases the penetration of wave energy deep into the shadow area remains underestimated in the phase-decoupled refraction–diffraction approximation.

5.3.2. Gap in infinite breakwater

Yu et al. (2000) observed the wave field in a compound of the above situation in a laboratory

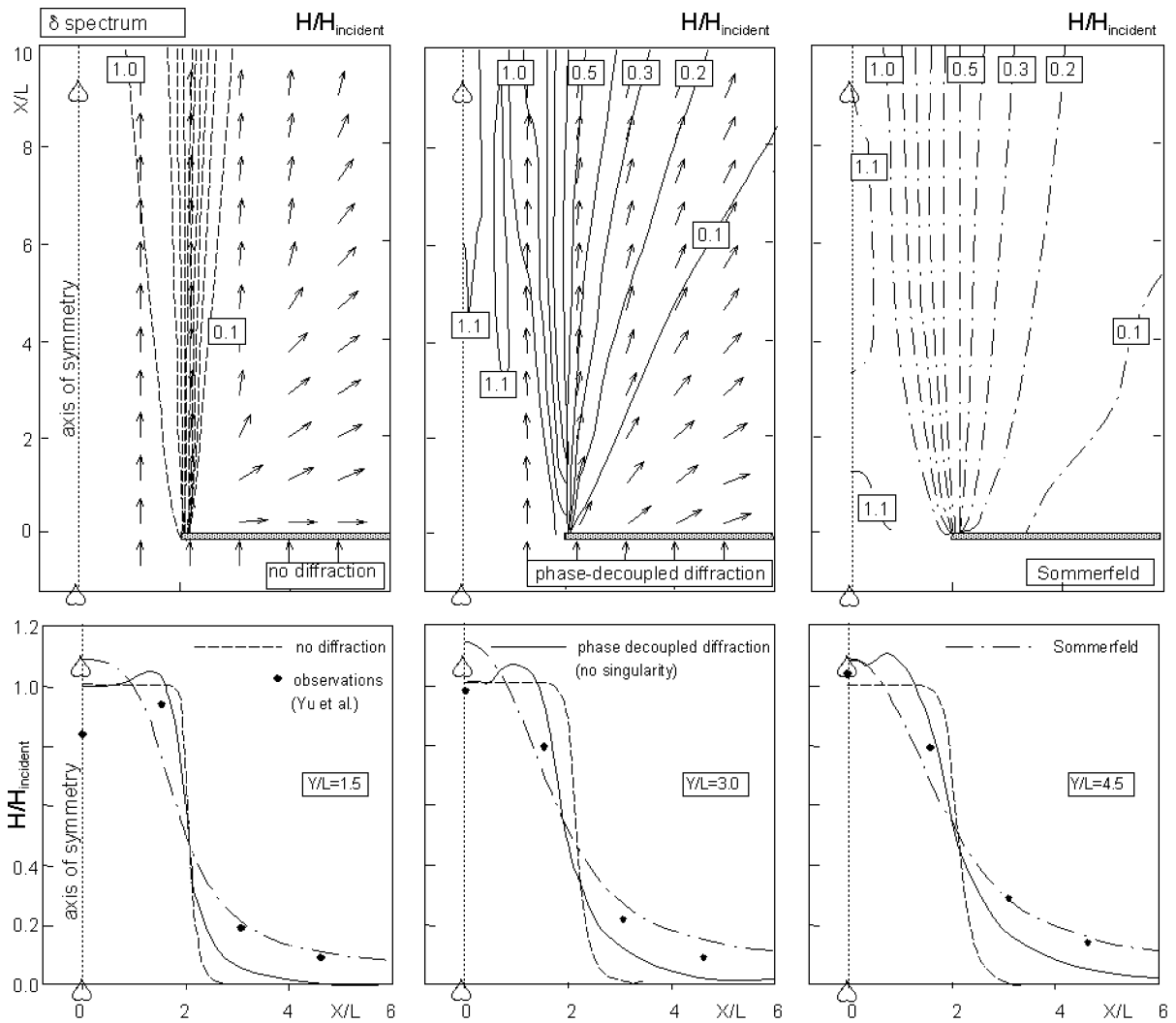


Fig. 5. Normalised wave height (local wave height divided by incident wave height) for unidirectional, monochromatic waves propagating in a tank from bottom to top (in this figure) through a gap in an “infinitely” long, straight breakwater. The computational results are shown for the right-hand half of the tank (line of symmetry indicated by  $\heartsuit$ - $\heartsuit$ ). Arrows indicate mean wave direction. Upper left panel=recti-linear propagation; upper centre panel=phase-decoupled diffraction (singularities accounted for in the computation), upper right panel=analytical Sommerfeld solution. Lower panels: comparison along transects and comparison with observations of Yu et al. (2000).

wave tank (a gap in an infinitely long, straight breakwater). The breakwater is a vertical wall (width=0.15 $L$ ) with rounded tips. The gap is  $4L$  wide (the wave length  $L=2$  m). The sides of the tank are absorbing, as is the up-wave side of the breakwaters. The incident waves are monochromatic and unidirectional (same  $\delta$ -spectrum as above) with the incident wave direction normal to the breakwater. Since the case is symmetrical around the centre line of the gap, the observations and computational results are shown in one half of the tank (Fig. 5). The wave field in this case can be estimated with the (complex) Sommerfeld solution of two semi-infinite breakwaters superimposed. It is remarkable that the Sommerfeld solution is close to the observations, except on the centre line of the gap where the Sommerfeld solution gives significantly higher wave heights than the observations.

It is obvious from the SWAN results (Fig. 5) that without diffraction, the SWAN results are poor, with the same characteristics as in the case of the semi-infinite breakwater. With the phase-decoupled refraction–diffraction approximation included (the singularity at the tip of the breakwater is *not* explicitly accounted for), SWAN reduces the differences with the Sommerfeld solution by about a factor 2. Remarkably, an overshoot off the central line is created in the phase-decoupled refraction–diffraction computation, which to some extent is supported by the observations (along the line  $y/L=1.5$ ; but

this observation is curiously far from the Sommerfeld solution).

## 6. Singularities

The computations have so far ignored the existence of the singularity at the tips of the breakwaters. To include these singularities in the computational model is not a trivial matter and we did not study this problem in depth. We only show here the significance of these singularities by using at the breakwater tip a much larger value of  $C_\theta$  than estimated in the above computations with the finite difference scheme (50 times larger; see section Numerical implementation). Comparing the results of the computations using this enhanced value of  $C_\theta$ , with the observations and the Sommerfeld solution of the gap in the breakwater shows that the results improve considerably, in particular in the deep shadow of the breakwater (Fig. 6). The computational results agree even slightly better with the observations than the Sommerfeld solution.

## 7. Discussion

The phase-decoupled refraction–diffraction approximation for spectral wave models that was used in this study is based on the mild-slope equation of Berkhoff (1972) but it has not been rigorously derived

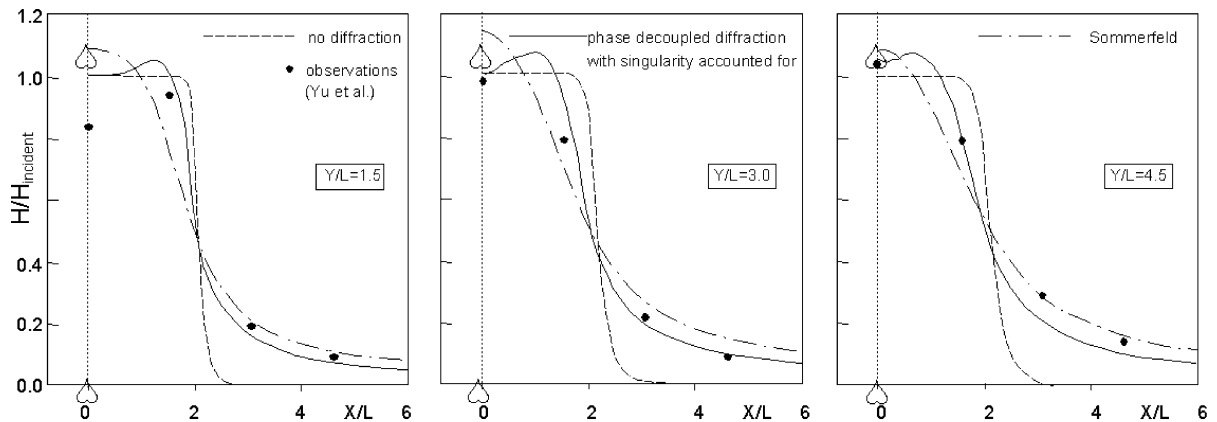


Fig. 6. Same as lower panels of Fig. 4. Singularities at the breakwater tips accounted for in the computation.

from that equation. That would require an investigation of a more fundamental nature. Instead, a reasonable assumption is made (replacing gradients of the normalised wave amplitude with gradients of the normalised square-root of the spectral density). Diffraction is thus formulated as an addition to the refraction-induced directional turning rate of the individual wave components in a continuous spectrum. The approximation has been coded with a central, second-order finite-difference technique in the iterative propagation schemes of the third-generation wave model SWAN (Booij et al., 1999).

The model has been verified in conditions that are more diffraction-prone than in the intended range of applications (verifications in small-scale conditions with monochromatic, long-crested waves versus applications in large-scale conditions with random, short-crested waves). But even in these extreme diffraction-prone conditions, the computational results agree reasonably well with observations and results of conventional refraction–diffraction models. The application of the approximation seems to be limited only by the required absence of phase-coupling in the wave fields (i.e., no coherent wave fields). In real conditions, such coherent wave fields may occur when the waves reflect in a coherent manner off a nearby obstacle or coastline (i.e., with deterministic phase-relationships between the incident wave field and the reflecting wave field). This implies that the phase-decoupled approximation should *not* be used if,

- (a) an obstacle or coastline covers a significant part of the down-wave view, *and in addition*,
- (b) the distance to the obstacle or coastline is small (less than a few wavelengths), *and in addition*,
- (c) the reflection off that obstacle or coastline is coherent, *and in addition*,
- (d) the reflection coefficient is significant.

(These are essentially the same criteria as for using parabolic refraction–diffraction models.) This implies that the phase-decoupled refraction–diffraction approximation of this study can be used in most situations, including situations near absorbing or reflecting coastlines of oceans, seas, bays, lagoons and fjords with an occasional obstacle such as islands, breakwaters, or headlands. It cannot be used in

harbours with standing waves or near well-defined cliff walls. Note that the coastline may be fully reflecting as long as the reflection is incoherent (e.g., irregular blocks, rocks or reefs that are small compared to the wave length) because incoherent reflection can be accounted for separately (it is in SWAN). A harbour with reflective quays that would induce coherent wave fields in the harbour (seen as standing wave patterns) cannot be accommodated.

The phase-decoupled refraction–diffraction approximation of the present study allows a separate evaluation of refraction and diffraction phenomena in specific cases. This can be achieved by de-activating the diffraction or refraction option in the code of the numerical model and inspect the effect in the computational results. This seems to be inherently impossible in Boussinesq models or models based on the mild-slope equation (the full mild-slope equation or the parabolic approximation). It is perhaps even more important that, with the phase-decoupled refraction–diffraction approximation it is possible to identify the areas in the computational domain where diffraction or refraction effects are induced. Such areas would be identified by high values of the refraction part of  $C_\theta$  (refraction–induction areas) or by high values of the diffraction part of  $C_\theta$  (diffraction–induction areas). This may help to select the proper model (refraction, diffraction, or a combination) to compute the wave field with more advanced propagation models if needed. In addition, it would help to determine in which areas of the computational domain the grid resolution should be high and in which areas it can be coarser. Alternatively, it may help to determine where nesting of models is required (possibly with different types of wave models).

Combining diffraction with refraction as in this study has many advantages, but more verification is required before any firm conclusion as to the applicability of the phase-decoupled refraction–diffraction approximation can be drawn. Our main but preliminary conclusion is that it seems to work reasonably well, at least for the intended range of applications (large-scale computations near an open coast with occasional obstacles). The problem of how to treat singularities in the computational domain, e.g. in the presence of breakwaters, is still unresolved. We do not suggest that the approach in the present study is correct. We merely showed that for monochromatic,

long-crested waves, a separate treatment of such singularities is required to obtain acceptable results in the deep shadow behind obstacles. It must be born in mind that spectral models are not intended to be used for such conditions.

The SWAN wave model that was used in the present study is a third-generation wave model for shallow water waves. The implementation of phase-decoupled diffraction in this model thus combines diffraction not only with refraction but also with processes of generation, dissipation, and wave–wave interactions, including wave–current interactions.

### Acknowledgements

We greatly appreciate comments of J.A. Battjes of the Delft University of Technology on an early version of the manuscript. We sincerely thank Y.S. Li of the Hong Kong Polytechnic University for providing us with the actual numbers of the observations of Yu et al. (2000) that were used in our study. The financial support of the US Office of Naval Research under Grant N00014-97-0113 is gratefully acknowledged.

### Appendix A

In the presence of an ambient current, the action balance equation is used rather than the energy balance equation. The action balance equation is:

$$\frac{\partial N}{\partial t} + \frac{\partial c_x N}{\partial x} + \frac{\partial c_y N}{\partial y} + \frac{\partial c_\sigma N}{\partial \sigma} + \frac{\partial c_\theta N}{\partial \theta} = \frac{S}{\sigma} \quad (1)$$

where the action density is  $N=N(\sigma,\theta)=E(\sigma,\theta)/\sigma$  (where  $\sigma$  is the relative frequency) and  $c_\sigma$  is the propagation speed in frequency space (Doppler shifting).

When diffraction is ignored, the expressions for the propagation speeds in the presence of an ambient current are (note that if diffraction is ignored, the separation parameter  $\kappa$  from  $\omega^2=g\kappa \tanh(\kappa d)$ , is equal to the wave number  $k=\kappa$ ):

$$\vec{c}_g = (c_x, c_y) = \frac{\vec{\kappa}}{\kappa} \frac{\partial \sigma}{\partial k} + \vec{U} \quad (2a)$$

$$c_\sigma = \frac{\partial \sigma}{\partial d} \left[ \frac{\partial d}{\partial t} + \vec{U} \cdot \nabla d \right] - c_g \vec{\kappa} \cdot \frac{\partial \vec{U}}{\partial s} \quad (2b)$$

$$c_\theta = - \left[ c_g \left( \frac{1}{\kappa} \frac{\partial \kappa}{\partial m} \right) + \frac{\vec{\kappa}}{\kappa} \cdot \frac{\partial \vec{U}}{\partial m} \right]. \quad (2c)$$

When diffraction is *not* ignored and the phase-decoupled approximation of this study is used, then the expressions are:

$$\vec{C}_g = \vec{c}_g (1 + \delta_E)^{1/2} + \vec{U} \quad (3a)$$

$$C_\sigma = \frac{\partial \sigma}{\partial d} \left[ \frac{\partial d}{\partial t} + \vec{U} \cdot \nabla d \right] - c_g \vec{\kappa} \cdot \frac{\partial \vec{U}}{\partial s} (1 + \delta_E)^{1/2} \quad (3b)$$

$$C_\theta = - \left[ c_g (1 + \delta_E)^{1/2} \left( \frac{1}{\kappa} \frac{\partial \kappa}{\partial m} + \frac{1}{2(1 + \delta_E)} \frac{\partial \delta_E}{\partial m} \right) + \frac{\vec{\kappa}}{\kappa} \cdot \frac{\partial \vec{U}}{\partial m} \right] \quad (3c)$$

in which all symbols have the same meaning as in the main text.

### References

- Battjes, J.A., 1968. Refraction of water waves. J. Waterw. Harb. Div., Proc. ASCE, New York, WW4, 437–451.
- Benoit, M., Marcos, F., Becq, F., 1996. Development of a third-generation shallow-water wave model with unstructured spatial meshing. Proc. 25th Int. Conf. Coastal Engineering. ASCE, New York, pp. 465–478.
- Berkhoff, J.C.W., 1972. Computations of combined refraction–diffraction. Proc. 13th Int. Conf. Coastal Engineering. ASCE, New York, pp. 471–490.
- Booij, N., 1981. Gravity waves on water with non-uniform depth and current. PhD Thesis. Delft University of Technology, Delft, the Netherlands. 130 pp.
- Booij, N., Holthuijsen, L.H., Doorn, N., Kieftenburg, A.T.M.M., 1997. Diffraction in a spectral wave model. Proc. 3rd Intl. Symposium Ocean Wave Measurement and Analysis WAVES 97. ASCE, New York, pp. 243–255.
- Booij, N., Ris, R.C., Holthuijsen, L.H., 1999. A third-generation wave model for coastal regions, Part I, model description and validation. J. Geophys. Res. 104 (C4), 7649–7666.
- Dingemans, M.W., 1997. Water wave propagation over uneven

- bottoms, Part 1-linear wave propagation. Adv. Ser. Ocean Eng., World Scientific 13 (471 pp.).
- Hasselmann, K., Barnett, T.P., Bouws, E., Carlson, H., Cartwright, D.E., Enke, K., Ewing, J.A., Gienapp, H., Hasselmann, D.E., Kruseman, P., Meerburg, A., Müller, P., Olbers, D.J., Richter, K., Sell, W., Walden, H., 1973. Measurements of wind-wave growth and swell decay during the Joint North Sea Wave Project (JONSWAP). Dtsch. Hydrogr. Z. Suppl. 12, A8.
- Holthuijsen, L.H., 1971. An investigation of two-dimensional wave propagation problems. MSc Thesis. Internal Report R1971/1/10. Delft University of Technology, Faculty of Civil Engineering, Fluid Mechanics Group. 67 pp.
- Komen, G.J., Cavaleri, L., Donelan, M., Hasselmann, K., Hasselmann, S., Janssen, P.A.E.M., 1994. Dynamics and Modelling of Ocean Waves. Cambridge Univ. Press, Cambridge. 532 pp.
- Kirby, J.T., 1986. Higher-order approximation in the parabolic equation method for water waves. J. Geophys. Res. 91 (C1), 933–952.
- Kuik, A.J., Van Vledder, G.Ph., Holthuijsen, L.H., 1988. A method for the routine analysis of pitch-and-roll buoy wave data. J. Phys. Oceanogr. 18 (7), 1020–1034.
- Lamb, H., 1932. Hydrodynamics, 6th ed. Dover Publications, New York. 738 pp.
- Li, Y.S., Zhan, J.M., 2001. Boussinesq-type model with boundary-fitted coordinate system. J. Waterw., Port, Coast., Ocean Eng., ASCE, New York, 127 (3), 152–160.
- Madsen, P.A., Sørensen, O.R., 1992. A new form of the Boussinesq equations with improved linear dispersion characteristics: Part 2. A slowly-varying bathymetry. Coast. Eng. 18, 183–205.
- Mase, H., Takayama, T., Kitano, T., 2001. Spectral wave transformation model with diffraction effect. Proc. 4th Int. Symposium Ocean Wave Measurement and Analysis, WAVES 2001, vol. 1. ASCE, New York, pp. 814–823.
- Mei, C.C., 1983. The Applied Dynamics of Ocean Surface Waves. Wiley, New York. 740 pp.
- Özkan, H.T., Kirby, J.T., 1993. Evolution of breaking directional spectral waves in the nearshore zone. Proc. 2nd Int. Conf. Ocean Wave Measurement and Analysis, WAVES'93. ASCE, New York, pp. 849–863.
- Panchang, V.G., Pearce, B.R., Briggs, M.J., 1990. Numerical simulation of irregular wave propagation over shoal. J. Waterw., Port, Coast., Ocean Eng., ASCE, New York, 116 (3), 324–340.
- Peregrine, D.H., 1966. Long waves on a beach. J. Fluid Mech. 27 (4), 815–827.
- Radder, A.C., 1979. On the parabolic equation method for water-wave propagation. J. Fluid Mech. 95 (1), 159–176.
- Resio, D.T., 1988. A steady-state wave model for coastal applications. Proc. 21st Int. Conf. Coast. Eng., ASCE, New York, pp. 929–940.
- Rivero, F.J., Arcilla, A.S., Carci, E., 1997. Analysis of diffraction in spectral wave models. Proc. 3rd Int. Symposium Ocean Wave Measurement and Analysis WAVES '97. ASCE, New York, pp. 431–445.
- Rogers, W.E., Kaihatu, J.M., Petit, H.A.H., Booij, N., Holthuijsen, L.H., 2002. Diffusion reduction in an arbitrary scale third generation wind wave model. Ocean Eng. 29, 1357–1390.
- Schönfeld, J.C., 1971. Propagation of Short Waves in Two Dimensions. Delft University of Technology, Delft, 12 pp., unpublished manuscript.
- Sommerfeld, 1896. Mathematische theorie der diffraktion. Mathematische Annalen 47, 317–374 (reference from Lamb, 1932).
- Vincent, C.L., Briggs, M.J., 1989. J. Waterw., Port, Coast., Ocean Eng., ASCE, New York, 115 (2), 269–284.
- Yu, Y.-X., S.-X., Li, Y.S., Onyx, Wai, W.H., 2000. Refraction and diffraction of random waves through breakwater. Ocean Eng. 27, 489–509.